RSC Advances

ROYAL SOCIETY
OF CHEMISTRY

www.rsc.org/advances

Controllable synthesis and enhanced microwave absorption properties of silane-modified

Ni$_{0.4}$Zn$_{0.4}$Co$_{0.2}$Fe$_2$O$_4$ nanocomposites covered with reduced graphene oxide

Peijiang Liu[a, b], Zhengjun Yao[a, b], Jintang Zhou[a, b]

[a]*College of Materials and Technology, Nanjing University of Aeronautics and Astronautics, Nanjing*

211100, Jiangsu, People's Republic of China

[b]*Jiangsu Key Laboratory of Advanced Structural Materials and Application Technology, Nanjing*

211100, Jiangsu, People's Republic of China

Correspondence to: Zhengjun Yao (E-mail: cz2343222@163.com Tel: +86 152 5181 6557)

Abstract

For the first time, silane coupling agent modified $Ni_{0.4}Zn_{0.4}Co_{0.2}Fe_2O_4$ ferrite covered with reduced graphene oxide nanocomposites were synthesized by a simple, efficient and controllable three-step method. The structural characteristics were investigated by Fourier transform infrared spectra, X-ray diffraction, elemental analysis, Thermal Gravity Analysis, field-emission scanning electron microscopy and transmission electron microscopy. The results indicated that the coupling agent modified ferrite particles were firmly and uniformly covered on the rGO nanosheets. Microwave adsorption properties were also performed at room temperature in the frequency range of 2-18 GHz. The minimum reflection loss of rGO/APTS–NZCF composites can reach −51.8 dB at 15.1 GHz with the thickness of 2.1 mm, and the effective bandwidth corresponding to R_L less than −10 dB was 5.3 GHz (from 12.7 to 18 GHz). The excellent microwave adsorption properties indicate this novel composite could be used as a new candidate for lightweight electromagnetic wave adsorption material.

Keywords: Reduced graphene oxide, Post-modification, nanocomposites, Microwave absorption property

1. Introduction

Considerable attention has been focused on microwave absorption materials because of their numerous applications in the fields of aero stealth technology, electromagnetic (EM) compatibility, environmental protection and communication facility.[1-6] Ideal microwave absorption materials are required to possess wide frequency bandwidth, minimum reflection loss (RL), antioxidant capability, good thermal stability and small thickness.[7-9] Among them, spinel ferrites have been utilized as one of the most promising candidate absorption materials in varied forms for many years due to their low cost, excellent magnetic loss, good stability and large resistivity.[10-12] However, in the microwave region, the

microwave absorption properties obtained by spinel ferrites are far below what is expected due to the

disadvantage of high density, which limits their industrial applications.

In order to reduce their high density and thickness, many new types of microwave absorption

ferrite materials with nano-sized additives have been studied since various nanomaterials were

discovered.[13-16] Compared with conventional nanomaterials, carbon based nanomaterials especially

graphene exhibit good absorption properties and electromagnetic interference (EMI) shieling effects

due to their low density and high dielectric loss.[17-23] Graphene and graphene-like nanomaterials coating

on the surface of ferrite particles may introduce dielectric loss to the nanocomposites. Furthermore, the

excellent electrical conductivity of graphene may produce skin effect and additional reflection at the

interface between air and composites, which can attenuate the electromagnetic wave effectively.

Therefore, considering the outstanding properties of graphene as well as ferrites, the combination of

magnetic materials and dielectric materials provides an effective way for electromagnetic shields to

absorb incident electromagnetic waves. A number of studies on microwave absorption and shielding of

ferrites containing graphene nanosheets have been reported in the previous papers. For example, Verma

et al.[24] investigated the microwave absorption properties of $BaFe_{12}O_{19}$@RGO nanocomposite, and they

found the total microwave absorption effectiveness can be achieved up to 32 dB in the Ku band

frequency range (12.4–18 GHz). Fu and his coworkers[25] synthesized $CoFe_2O_4$ hollow sphere/graphene

composites. The results exhibited that the minimum reflection loss (RL) of composite at a thickness of

2.0 mm reached −18.5 dB, and the effective absorption bandwidth was 3.7 GHz. However, there are

some critical issues in constructing composites of ferrites and graphene nanosheets. Ferrite particles are

easily subjected to strong magnetic attractive forces between nanoparticles, which result in aggregation

on the surface of graphene substrate. So it's a big challenge to disperse ferrite particles uniformly on

graphene nanosheets without obvious aggregation. Recently, surface chemical modification of ferrite particles known as the core-shell structure, is regarded as an effective way to decrease interparticle magnetic forces leading to uniform dispersion.[26, 27] In light of this, the introduction of surface modified ferrite with coupling agent onto the graphene substrate may largely improve the compatibility, mechanical property and microwave absorption property because coupling agent can act as a molecular bridge between two incompatible phases by formation of physical and chemical interactions between inorganic ferrite particles and graphene nanosheets. To the best of our knowledge, there are few studies on the controlled synthesis of coupling agent modified ferrite covered with graphene nanosheet, which may have excellent microwave absorption properties.

In the present work, the cubic $Ni_{0.4}Zn_{0.4}Co_{0.2}Fe_2O_4$ (NZCF) ferrite particles were synthesized through the sol-gel autoignition method, and then post-modified by 3-aminopropyltriethoxy silane (APTS). The thermal reduced graphene oxide (rGO)/APTS–NZCF nanocomposites were obtained by the ultrasonic and mechanical blending. The morphology and structure were characterized and analyzed in detail. Furthermore, the soft magnetic property, complex permittivity, permeability and microwave absorption of the rGO/APTS–NZCF nanocomposites were also investigated. It is believed that such novel materials may find applications in microwave absorption fields.

2. Experimental section

2.1 Materials

Nickel nitrate ($Ni(NO_3)_2 \cdot 6H_2O$), zinc nitrate ($Zn(NO_3)_2 \cdot 6H_2O$), cobalt nitrate ($Co(NO_3)_2 \cdot 6H_2O$), ferric nitrate ($Fe(NO_3)_3 \cdot 9H_2O$), 3-aminopropyltriethoxy silane (APTS) and citric acid were commercially purchased from Aladdin Chemical Reagent, China. Graphite oxide used in this work was prepared from natural graphite powder (Sinopharm Chemical Reagent) according to the modified

Hummers and Offeman's method.[28] Unless otherwise stated, all chemical reagents in this work were of analytical grade and used as raw materials without further purification.

2.2 Preparation of reduced graphene oxide and $Ni_{0.4}Zn_{0.4}Co_{0.2}Fe_2O_4$ ferrite

To get graphene oxide (GO), the graphite oxide powders were dispersed into ether by mild ultrasonication over 2 h, and the solution was dried in a vacuum oven at room temperature for 24 h. Then the GO was heated in a vacuum oven from room temperature to 450 ^{o}C, isothermal heating for 10 min, to obtain the reduced graphene oxide.

Ferrite particles were synthesized by the conventional nitrate citric acid sol-gel autoignition method, and the molar ratio of $Ni^{2+}:Zn^{2+}:Co^{2+}:Fe^{3+}$ is about 0.4:0.4:0.2:2, which gives a composition of $Ni_{0.4}Zn_{0.4}Co_{0.2}Fe_2O_4$. The detailed preparation procedure is as follows: $Ni(NO_3)_2\cdot6H_2O$ (5 mmol), $Zn(NO_3)_2\cdot6H_2O$ (5 mmol), $Co(NO_3)_2\cdot6H_2O$ (2.5 mmol), $Fe(NO_3)_3\cdot9H_2O$ (25 mmol) and citric acid (37.5 mmol) were added into the deionized water (60 mL) to form a clean solution with magnetic stirring. Subsequently, the ammonia solution was added dropwise to the suspension to adjust the pH value to 6. After that, the suspension was heated to 80 ^{o}C and stirred vigorously for 6 h. The obtained brown dried gels were put into a digital oven, and the temperature maintained at 200 ^{o}C for another 2 h. Then, the dried gels were auto-ignited in order to obtain loose powders. Finally, the powders were calcinated at 1080 ^{o}C for 4 h to decompose all the organic components and then the as-prepared NZCF ferrite was obtained by slowly cooling to room temperature.

2.3 Preparation of ferrite particles coated with APTS

NZCF particles were modified with APTS by a self-assembly process (Fig. 1). For example, 0.5 g ferrite was suspended in a 100 mL ethanol solution with a 95:5 volume ratio of ethanol and deionized water. The NH_4OH was then added drop by drop to the suspension to adjust the pH value to 4. The

solution was sonicated for 1 h and mechanically stirred for 5 h at 60 °C. Subsequently, the target

particles were separated by filtration, washed 3 times with absolute alcohol and heated at 60 °C for over

12 h.

2.4 Preparation of rGO/APTS–NZCF nanocomposites

The rGO/APTS–NZCF composites were prepared in the following steps: APTS–NZCF particles

and rGO with a weight ratio of 15:1 were added to an absolute ethanol medium, followed by

ultrasonication and stir for 12 h. Then the solution was dried at 60 °C under vacuum to obtain final

composites. Compared with the reported in-situ methods,[17, 25, 29] the preparations of APTS–NZCF

particles and rGO/APTS–NZCF nanocomposites occur step by step, thus making the process much

safer and more controllable. For comparison, a reference rGO/NZCF nanocomposite was also

synthesized in a similar way. The detailed route of a controllable two-step method for preparing the

rGO/APTS–NZCF composites is schematically illustrated in Fig. 1.

2.5 Characterization

The chemical structures of samples were characterized by Fourier transform infrared spectra

(FT-IR) using a spectrometer (Bruker Vertor 33) in the range of 4000-500 cm^{-1}. The elemental

composition was confirmed by CHNS elemental analysis (Analytik Jena AG EA3000). A

high-resolution X-ray photoelectron spectrometer (XPS) (Thermo ESCALAB 250Xi, USA) was used

to investigate the presence of surficial elements with Al Kα radiation of 1486.6 eV. The crystalline

phase structure of composites were confirmed by X-ray powder diffraction (XRD) using a Bruker-D8

DISCOVER X-ray diffractometer (Cu Kα radiation with λ = 1.5406 BRUKER, US) in the scattering

range (2θ) of 10-80° at an accelerated voltage of 40 kV. A thermogravimetric analyzer (QUANTA-200)

was used to measure the thermal stability of the samples under air atmosphere in the temperature range

of 25–900 $^{\circ}$C at a heating rate of 10 $^{\circ}$C/min. The particle size and the surface morphology of the rGO, APTS–NZCF particles and nanocomposites were examined using field emission scanning electron microscopy (FE-SEM, Hitachi S-4800N) and Transmission electron microscopic (TEM, Tecnai 12). The composition analysis of the composites was performed by energy dispersive spectra (EDS). For the measurement of microwave absorption properties, the samples were homogeneously dispersed in paraffin matrix with a 7:3 weight ratio of sample and paraffin. The mixture was then pressed into toroidal with a dimension of 3 mm in inner diameter, 7 mm in outer diameter and 2.0-2.5 mm in thickness. Then the samples were inserted into a copper holder and connected between the waveguide flanges of the network analyzer. The electromagnetic parameter and reflection loss of the composites were measured by Agilent PNA N5224A vector network analyzer using the coaxial-line method in the frequency range of 2–18 GHz.

3. Result and discussion

3.1 Structural characterization of samples

In our paper, the rGO nanosheets were prepared by the thermal reduction process of GO sheets. As we all know, the nanosheet of GO is covered mostly with oxygen–containing functional groups such as carbonyl, carboxyl, epoxide and hydroxyl groups.[30, 31] These groups can destroy the big π conjugations over the graphene sheet, which leads to attenuation of the electronic properties.[31] Thus, it's very important to eliminate the oxygen–containing functional groups, and the relevant process is named deoxygenation. In this work, X–ray photoelectron spectroscopy (XPS) was used to characterize the surficial elemental composition of samples and to detect the extent of reduction of GO. As shown in Fig. 2a, the C 1s XPS spectrum of GO can be deconvoluted into six peaks centered at 284.5, 285.1, 286.7, 287.0, 287.6 and 289.0 eV, corresponding to C=C bond, C–C bond, C–OH bond, epoxy/ether C–

O–C, carbonyl C=O and carboxylate O–C=O groups of graphene oxide, respectively.[32-34] Compared

with GO (in Fig. 2b), the XPS spectrum of rGO also exhibits similar oxygen functionalities originating

from GO. However, the peak intensities of C–OH, C–O–C, C=O and O–C=O groups decrease

obviously, which demonstrates a considerable degree of reduction. In addition, small amounts of

oxygen–containing functional groups which remain on the surface of rGO sheets can promote the

mutual compatibility between rGO and chemical modified ferrite particles.

To investigate the formation of APTS–NZCF particles on rGO, XRD patterns of rGO, pure NZCF

and rGO/APTS–NZCF hybrids are shown in Fig. 3. For rGO nanosheets, the reduction of GO is

confirmed by its weak and broad diffraction peak at $2\theta = 24.5^{\circ}$ ascribed to the (002) reflection plane of

graphene sheet, indicating that most of these oxygen–containing functional groups on the surface of

GO are removed effectively during the thermal reduction process. The result reveals the typical

amorphous carbon nature of rGO. In the case of NZCF particles, there are nine major peaks at angles

($2\theta = 18.40^{\circ}$, 30.22°, 35.58°, 37.22°, 43.24°, 53.60°, 57.14°, 62.72° and 74.16°), which can be well

indexed to the (111), (220), (331), (222), (400), (422), (511), (440) and (533) planes, respectively,

demonstrating the typical spinel structure (space group $Fd3m$) of NZCF. All the observed diffraction

peaks are well matched with the standard reference data (JCPDS, PDF no. 04–009–3215). The sharp

diffraction peaks and high intensity exhibit the good crystallinity of the ferrite particles. The

rGO/APTS–NZCF nanocomposite shows the retained characteristic peaks of NZCF ferrite and a slight

shift in 2θ in comparison to the diffraction peaks of pure ferrite, which demonstrates the proper

interaction between rGO nanosheets and APTS–NZCF particles.[35] However, no obvious diffraction

peak ascribed to rGO is observed, indicating that the adsorption of NZCF ferrite on the surface of rGO

sheet destroy the regular layer stacking of graphene.[25]

Fig. 4a shows the typical FT-IR spectra of pure NZCF, APTS–NZCF particle and rGO/APTS–

NZCF hybrid composite in the wave number range of 400–4000 cm^{-1}. The FT-IR spectrum of NZCF

particle shows characteristic peaks at 540–600 cm^{-1} and 400–460 cm^{-1}, which are due to the lattice

stretching vibrations of oxygen and cations at octahedral and tetrahedral positions, confirming that

$Ni_{0.4}Zn_{0.4}Co_{0.2}Fe_2O_4$ ferrite are formed. In addition, the peak at 1630 cm^{-1} corresponds to the O–H

bending vibration. For NZCF particle, there are plenty of bare atoms such as Ni, Zn, Co, Fe and O on

the particle surface, which would adsorb OH$^-$ to form hydroxyl-rich surface. The –OH on the surface

can further react with APTS as the reaction process shown in Fig. 1. Therefore, the magnetite NZCF

can be coated with APTS coupling agent by chemical bond. The structural changes are proved by

FT-IR spectrum. As shown in Fig. 4a, compared with the pure NZCF, the APTS modified NZCF

particle possesses a band in 1386 cm^{-1} assigned to the stretching vibration of –CN bond, a broad

absorption band in 1087 cm^{-1} assigned to the stretching vibration of SiO–H and Si–O–Si bonds and a

weak band in 877 cm^{-1} assigned to the bending vibration of –NH$_2$ bond. These results reveal the

existence of APTS on ferrite surface. In addition, the characteristic band of Fe–O–Si bond can't be

observed in the spectrum because it appears at around 584 cm^{-1} and thus overlaps with the Fe–O

stretching vibration of ferrite particles. In the case of rGO/APTS–NZCF nanocomposite, the new peak

at 1727 cm^{-1} corresponding to the stretching vibration of C=O bond appears with the addition of rGO.

Compared with APTS–NZCF particle, there is a slight blue-shift of the peak at 1630 cm^{-1} for

rGO/APTS–NZCF nanocomposite, which may be caused by the skeletal vibration of graphene

nanosheets.[24] Furthermore, according to the previous paper,[36-38] it can form chemical bonding easily

between rGO nanosheets and APTS molecules (as shown in Fig. 1). However, in the FT-IR spectrum of

rGO/APTS–NZCF composite, we can't figure out the characteristic peak of –NHCO– which is

obtained by the reaction of –COOH group and –NH$_2$ group. It is because that the characteristic peak of

amide carbonyl-stretching mode overlaps with that of O–H bending vibration at 1630 cm^{-1}, and

furthermore, the total amount of –COOH bonds on the surface of rGO is very limited, which makes the

characteristic peak remain unchanged. The elemental analysis of rGO/APTS–NZCF composites

observed in inset of Fig. 4 was used to characterize amide bonding. According to the content of

nitrogen, it can be assumed that about 0.86 wt% of –NHCO– is generated on the surfaces of graphene

nanosheets. Thus, the APTS modified NZCF particle has been incorporated onto the rGO surface

successfully, and there are some chemical interactions between APTS–NZCF and rGO.

Fig. 1 shows the possible interaction mechanism between APTS–NZCF particle and rGO

nanosheet. In addition to the chemical bonding between the two components, electrostatic interaction is

another main reason to connect ferrite and rGO. As illustrated in other researches,[19, 31] the ferrite

particles which possess positive charge can be attached to the negatively charged rGO sheets through

physical electrostatic adsorption. So it can be concluded that the coupling agent modified ferrites are

firmly and uniformly dispersed on the surface of rGO by both the chemical bonding and physical

electrostatic.

In order to investigate the amount of APTS–NZCF particles supported on rGO nanosheets, the

thermogravimetric tests of the as-prepared samples were carried out from 25 to 900 ^{o}C in air

atmosphere. As presented in Fig. 5, Ni$_{0.4}$Zn$_{0.4}$Co$_{0.2}$Fe$_2$O$_4$ particles, with extraordinary high thermal

stability, show nearly no weight loss over the entire temperature range. For rGO nanosheets, there is a

small proportion of weight loss below 450 ^{o}C but drops dramatically with the increasing of temperature

from 450 to 560 ^{o}C, which is ascribed to the oxidation of carbon.[17] The residual weight of rGO is about

4.6 wt%, indicating that rGO is completely combusted. In case of rGO/APTS–NZCF composite, the

main weight loss at 450–580 $^{\circ}$C is supposedly due to the decomposition of rGO. In addition, the

residual weight for composite is about 94.2 wt% at 580 $^{\circ}$C. From the results of thermal gravity analysis

and elemental analysis, we can conclude that the weight ratios of APTS–NZCF particles and rGO

nanosheets in the composites are about 94.8 wt% and 5.2 wt%, respectively.

3.2 Morphological characterization

The APTS modified NZCF particles can exhibit a strong magnetization in the presence of a

magnetic field due to the inherent properties of the magnetic particles. Thus, the nanocomposite with a

certain amount of rGO should inherit the magnetic properties. As shown in Fig. 6a, the obtained

nanocomposites which present a good magnetic response are easily attracted by a permanent magnet in

ethanol solution. Even after sonication for a long time, the rGO/APTS–NZCF nanocomposites were

still stability anchored on the surface of rGO, and no obvious rGO nanosheets are dispersed outside of

the nanocomposite, indicating the strong interaction between the two components.

Typical FE-SEM images of rGO, pure NZCF, APTS–NZCF particle and rGO/APTS–NZCF

nanocomposite are shown in Fig. 6b-e. It is found from Fig. 6b that the rGO exhibits thin sheet

structure with wrinkled, folded and silk-like morphology. Furthermore, the rGO nanosheets appear as

an isolated lamellar structure and a random distribution, which are convenient for magnetic particle to

anchor on the large surface of rGO. In the case of pure NZCF, the magnetic particles have a typical

cubic geometrical morphology with sizes ranging from 100 to 500 nm as shown in Fig. 6c. The outlines

of the pure NZCF particles are clear and distinct. However, when coupling agent was introduced to the

ferrite material, the outlines of APTS–NZCF particles become blurry and obscure (Fig. 6d). This may

be considered as an indirect evidence that magnetic ferrite is successfully modified by silane coupling

agent. In addition, both pure NZCF particles and APTS–NZCF particles are polydisperse and these

particles have a tendency to form agglomeration due to the magnetic dipole interactions between powders. Fig. 6e shows the morphology of rGO/APTS–NZCF nanocomposites. It can be seen that APTS–NZCF particles are homogeneously distributed on the surface of the two dimensional rGO nanosheets, demonstrating a strong interaction between rGO and ferrite. However, the small NZCF particles still tend to agglomerate on the rGO surface because of the powerful inherent magnetic interaction of ferrite particles. The EDS curve of APTS modified NZCF particle is shown in Fig. 6f. The result suggests the stoichiometric composition of as-synthesized NZCF ferrite, with average errors Fe 7.2%, Zn 1.4%, Ni 1.4% and Co 0.7%, and it further confirms that the coupling agent have been grafted on the surface of ferrite successfully. In addition, the peak of Si exhibits strong intensity, which may be caused by the monocrystalline silicon chip.

Fig. 7 demonstrates TEM micrographs of rGO and rGO/APTS–NZCF nanocomposite. It can be clearly seen in Fig. 7a that rGO nanosheets display an ultrathin, wrinkled silk-like morphology, suggesting the full exfoliation of rGO sheets. For the rGO/APTS–NZCF nanocomposite in Fig. 7b, the modified NZCF particles are uniformly distributed on the surface and edge of rGO or wrapped by adjacent rGO nanosheets like a sandwich structure in some blurry areas, indicating a firm interaction between the two materials, which may bring some advantages for microwave adsorption properties.[24]

3.3 Magnetic properties

The magnetic properties of the as-synthesized $Ni_{0.4}Zn_{0.4}Co_{0.2}Fe_2O_4$ and rGO/APTS–NZCF nanocomposite were measured using a vibrating sample magnetometer (VSM) with an external field – 70 kOe $\leq$ H $\leq$ 70 kOe at room temperature and the measurement results are presented in Fig. 8. Magnetic characteristics suggest a mixed state of ferrimagnetic and superparamagnetic behavior in the NZCF particles.[39, 40] It is found that the saturation magnetization (M_s) for NZCF is 84.1 emu/g, and the

coercive field (H_c) is very less. High value of M_s along with the low value of H_c may be productive for soft magnetic applications.[39] A similar behavior for the rGO/APTS–NZCF nanocomposites is observed. The saturation magnetization for rGO/APTS–NZCF has decreases slightly (75.7 emu/g), but is still quite high. The smaller value of M_s is attributed to the existence of nonmagnetic rGO and APTS in the nanocomposites.

3.4 Microwave absorption properties

A vector network analyzer was employed to investigate the complex permittivity ($\varepsilon_r = \varepsilon' - j\varepsilon''$) and complex permeability ($\mu_r = \mu' - j\mu''$) of samples in the frequency range of 2–18 GHz. As we all know, the term ε' and μ' are associated with storage ability of electromagnetic energy, and the ε'' and μ'' are associated with the dissipation of energy, which results from conduction, resonance and relaxation mechanisms.[41] Fig. 9 shows the frequency dependence on the basic electromagnetic parameters of the rGO, pure NZCF, rGO/NZCF and rGO/APTS–NZCF nanocomposite. It can be observed that there are some obvious fluctuations in the real part ε' for rGO nanosheet, which may be due to the leakage conductance and lags of polarization in low frequency, and the interfacial polarization and associated relaxation in high frequency. The ε' and ε'' values of the rGO/NZCF and rGO/APTS–NZCF nanocomposite decrease gradually with the increase of frequency in the range of 2–18 GHz. Moreover, The ε' and ε'' of nanocomposites are lower than those of rGO nanosheets and higher than those of pure NZCF particles, which is ascribed to the high electric conductivity of rGO. Furthermore, the addition of rGO in magnetic materials can increase the interfaces of nanocomposites, and then lead to the accumulation of virtual charges on the interfaces of two substrates with different dielectric constants, which enhances the dipole and interfacial polarization and is known as Maxwell-Wagner polarization.[42] This phenomenon can also improve the dielectric constant. For pure NZCF particle, the ε' and ε''

values keep a stable constant. The dielectric loss tangent is calculated based on the ratio of the imaginary part to the real part ($\varepsilon''/\varepsilon'$), which is represented by $\tan\delta_\varepsilon$. As presented in Fig. 9c, the dielectric loss of rGO/APTS–NZCF is greater than that of rGO/NZCF in the whole frequency range. According to a recent research,[26] the dielectric loss is attributed to the dispersion of ferrite particles in the substrate. For the coupling agent modified ferrite, as the above SEM and TEM shown, the uniform distribution of NZCF particles on rGO nanosheets provides more free ionic, dipole and interfacial polarization leading to considerable contribution to complex permittivity.

The relative complex permeability parameters of samples are illustrated in Fig. 9d-f. For rGO, the values of μ' and μ'' almost keep constant below 10 GHz and begin to intensively fluctuate with frequency increase. In the case of pure NZCF, rGO/NZCF and rGO/APTS–NZCF nanocomposite, the complex permeability parameters (μ' and μ'') decrease gradually with the increase of frequency in the same manner. The APTS modified ferrite particles coated by rGO show a lower value of real part (μ') than the original rGO/NZCF composites in the whole frequency range. In addition, the value of imaginary part (μ'') of rGO/APTS–NZCF is higher in low frequency range compared with that of rGO/NZCF. The phenomenon can be attributed to the fine dispersion, which reduces the magnetic energy storage capability of NZCF particles and increases the domain wall resonance and spin rotation.[43] We have also calculated the magnetic loss tangent ($\tan\delta_\mu = \mu''/\mu'$) of the samples, shown in Fig. 9f. It can be seen that the maximum peak of the magnetic loss tangent for rGO/APTS–NZCF nanocomposite appears at 5.7 GHz, and the peak values is 0.86.

The microwave adsorption properties of the samples can be represented by the reflection loss (R_L), which can be further calculated from the obtained complex permittivity and complex permeability parameters by the given absorber thickness and frequency according to the transmission line theory[44]

using the following equation:

$$R_L(dB) \;=\; 20\log\left|\left(Z_{in} - 1\right)/\left(Z_{in} + 1\right)\right| \tag{1}$$

$$Z_{in} \;=\; \sqrt{\mu_r/\varepsilon_r}\,\tanh\left[j\left(2\pi fd/c\right)\sqrt{\varepsilon_r\mu_r}\right] \tag{2}$$

where Z_{in} is the normalized input impedance of the absorber in free space, d is thickness of the absorb

layer, c is the velocity of EM waves in free space and f is the microwave frequency.

The calculated reflection losses of nanocomposites are shown in Fig. 10. As revealed in Fig. 10a,

when the thickness of the absorb layer is 2 mm, the minimum R_L of rGO/APTS–NZCF nanocomposite

reaches −33.9 dB at 15.8 GHz, which is greater than −24.8 dB at 14.8 GHz of rGO/ NZCF

nanocomposite, and the bandwidth corresponding to R_L less than −10 dB (90% of microwave

absorption) can reach 4.5 GHz (from 13.5 to 18.0 GHz). The better microwave adsorption properties of

modified nanocomposite are attributed to not only the synergistic effect of the modified ferrite particles

and rGO nanosheets but also the improved interfacial compatibility between the rGO and modified

NZCF. Fig. 10b exhibits the three-dimensional illustration of calculated reflection loss curves of the

rGO/APTS–NZCF nanocomposite at various thicknesses (1–5 mm) in the frequency range of 2–18

GHz. It can be observed that the minimum R_L value of rGO/APTS–NZCF is about −51.8 dB at 15.1

GHz with the thickness of 2.1 mm, and the corresponding adsorption frequency bandwidth ($R_L < -10$

dB) can reach 5.3 GHz (from 12.7 to 18 GHz). It is worth noting that the adsorption peaks have a trend

to shift toward the low frequency areas as the thickness of the material increase from 1.0 to 5.0 mm,

and the minimal R_L value decreases simultaneously. All the above results apparently indicate that the

rGO/APTS–NZCF nanocomposites exhibit a better adsorption performance and a broader bandwidth

with a thinner thickness than the unmodified NZCF composites and other graphene-ferrite composites,

such as rGO/Fe_3O_4 composites (−26.4 dB at 5.3 GHz with a thickness of 5 mm),[45] $CoFe_2O_4$ hollow

sphere/graphene composites (−18.5 dB at a thickness of 2.0 mm),[25] cubic-$NiFe_2O_4$/graphene-polyaniline composites (−50.5 dB at 12.5 GHz with a thickness of 2.5 mm) [46] and rugby-shaped $CoFe_2O_4$/graphene composites (−39.0 dB at a thickness of 2 mm).[47] Therefore, the rGO/APTS–NZCF nanocomposites can effectively serve as new types of potential microwave adsorption materials in the frequency range from 2 to 18 GHz.

Generally, the dielectric loss, magnetic loss and the complementarities between the two losses are of great importance to microwave adsorption properties. So, the excellent microwave adsorption intensities and wider adsorption bandwidths of rGO/APTS–NZCF nanocomposites can be explained as follows: Firstly, there exist a lot of multi-interfaces between rGO nanosheets and modified NZCF particles, resulting in the increase of interfacial polarization and the associated relaxation, which causes the enhancement of dielectric loss. Furthermore, according to the recent research results, charges can transfer through the interface of a graphene-ferrite heterostructure because of their different physic properties.[48] Therefore, in present work, a charge transfer process would reasonably occur in the interface between rGO and modified ferrite, and free carriers are introduced from ferrite into graphene, which give rise to the electric polarization in the nanocomposites. This process can also make great contribution to the increase of dielectric loss. Secondly, the magnetic loss of rGO/APTS–NZCF nanocomposites, originating from the outstanding magnetic properties of the NZCF particles, plays an important role in enhancing the adsorption. The magnetic loss mainly stems from hysteresis loss, domain wall resonance, natural resonance and eddy current effect. For the ferrite composite absorber, the eddy current effect often occurs in the high frequency range, and can be related to the values of C_0 ($C_0 = \mu''(\mu')^{-2}f^{-1}$). If the eddy current effect is the main loss mechanism, the value of C_0 should be a constant even when the frequency changes.[46] As presented in Fig. 11, the values of C_0 dramatically

decrease from in the frequency range from 2 to 14 GHz, and then keep constant after 14 GHz. That is to say, the magnetic loss of rGO/APTS–NZCF nanocomposite, with a peak at 5.6 GHz, is mainly caused by the natural resonance and exchange resonance, and the magnetic losses in the frequency range of 14–18 GHz are caused by eddy current effect. Finally, the coupling agent modified nanocomposites provide more dipole polarization, interfacial polarization, domain wall resonance and spin resonance than the unmodified nanocomposites, which can greatly improve the adsorption properties.

4. Conclusion

In summary, the rGO/APTS–NZCF nanocomposites were successfully prepared by a simple, safe and controllable three-step method. The structural characteristics of composites were investigated by FT-IR, XRD, elemental analysis, TGA, SEM and TEM, and the results indicated that the coupling agent modified ferrite particles were firmly and uniformly covered on the rGO nanosheets. In addition, the measurements of microwave adsorption properties revealed that the minimum reflection loss of rGO/APTS–NZCF composites can reach –51.8 dB at 15.1 GHz with the thickness of 2.1 mm, and the effective bandwidth corresponding to R_L less than –10 dB was 5.3 GHz (from 12.7 to 18 GHz). Therefore, the rGO/APTS–NZCF composites will be attractive candidates for microwave adsorption materials.

Acknowledgements

References

1. A. Baniasadi, A. Ghasemi, A. Nemati, M. Azami Ghadikolaei and E. Paimozd, *J Alloy Compd*, 2014, **583**, 325-328.
2. H. M. Khan, M. U. Islam, Y. Xu, M. Asif Iqbal and I. Ali, *J Alloy Compd*, 2014, **589**, 258-262.
3. C. H. Peng, C. C. Hwang, J. Wan, J. S. Tsai and S. Y. Chen, *Materials Science And Engineering B-Solid State Materials for Advanced Technology*, 2005, **117**, 27-36.
4. S. P. Ruan, B. K. Xu, H. Suo, F. Q. Wu, S. Q. Xiang and M. Y. Zhao, *J Magn Magn Mater*, 2000, **212**, 175-177.
5. D.-L. Zhao, Q. Lv and Z.-M. Shen, *J Alloy Compd*, 2009, **480**, 634-638.
6. P. Liu, Z. Yao and J. Zhou, *Ceram Int*, 2015, **41**, 13409-13416.
7. H. Yang, M. Cao, Y. Li, H. Shi, Z. Hou, X. Fang, H. Jin, W. Wang and J. Yuan, *Advanced Optical Materials*, 2014, **2**, 214-219.
8. M.-S. Cao, J. Yang, W.-L. Song, D.-Q. Zhang, B. Wen, H.-B. Jin, Z.-L. Hou and J. Yuan, *Acs Appl Mater Interfaces*, 2012, **4**, 6949-6956.
9. X.-J. Zhang, G.-S. Wang, W.-Q. Cao, Y.-Z. Wei, J.-F. Liang, L. Guo and M.-S. Cao, *Acs Appl Mater Interfaces*, 2014, **6**, 7471-7478.
10. A. Tadjarodi, R. Rahimi, M. Imani, H. Kerdari and M. Rabbani, *J Alloy Compd*, 2012, **542**, 43-50.
11. O. Yalçın, H. Bayrakdar and S. Özüm, *J Magn Magn Mater*, 2013, **343**, 157-162.
12. P.-J. Liu, D.-S. Ma, D. Xiao and G.-F. Hou, *Inorg Chem Commun*, 2013, **33**, 158-160.
13. F. Wen, N. Wang and F. Zhang, *Solid State Commun*, 2010, **150**, 1888-1891.
14. A. Sharbati, J. Mola Verdi Khani and G. R. Amiri, *Solid State Commun*, 2012, **152**, 199-203.
15. P. Talbot, A. M. Konn and C. Brosseau, *J Magn Magn Mater*, 2002, **249**, 481-485.
16. M. Mishra, A. P. Singh, B. P. Singh, V. N. Singh and S. K. Dhawan, *Journal Of Materials Chemistry A*, 2014, **2**, 13159-13168.
17. P. Liu, Y. Huang and X. Zhang, *Compos Sci Technol*, 2015, **107**, 54-60.
18. M. Zong, Y. Huang, H. Wu, Y. Zhao, Q. Wang and X. Sun, *Mater Lett*, 2014, **114**, 52-55.
19. M. Zong, Y. Huang, X. Ding, N. Zhang, C. Qu and Y. Wang, *Ceram Int*, 2014, **40**, 6821-6828.
20. T. K. Gupta, B. P. Singh, V. N. Singh, S. Teotia, A. P. Singh, I. Elizabeth, S. R. Dhakate, S. K. Dhawan and R. B. Mathur, *Journal Of Materials Chemistry A*, 2014, **2**, 4256-4263.
21. L. Wang, Y. Huang, X. Sun, H. Huang, P. Liu, M. Zong and Y. Wang, *Nanoscale*, 2014, **6**, 3157-3164.
22. A. P. Singh, M. Mishra, P. Sambyal, B. K. Gupta, B. P. Singh, A. Chandra and S. K. Dhawan, *Journal Of Materials Chemistry A*, 2014, **2**, 3581-3593.
23. L. Wang, Y. Huang, C. Li, J. Chena and X. Sun, *Phys Chem Chem Phys*, 2015, **17**, 5878-5886.
24. M. Verma, A. P. Singh, P. Sambyal, B. P. Singh, S. K. Dhawan and V. Choudhary, *Phys Chem Chem Phys*, 2015, **17**, 1610-1618.
25. M. Fu, Q. Jiao, Y. Zhao and H. Li, *Journal Of Materials Chemistry A*, 2014, **2**, 735-744.
26. W. Wang, C. Zang and Q. Jiao, *J Magn Magn Mater*, 2015, **378**, 261-266.
27. Q. Dai, M. Lam, S. Swanson, R.-H. R. Yu, D. J. Milliron, T. Topuria, P.-O. Jubert and A. Nelson, *Langmuir*, 2010, **26**, 17546-17551.
28. W. S. Hummers and R. E. Offeman, *J Am Chem Soc*, 1958, **80**, 1339-1339.
29. S. Bai, X. Shen, X. Zhong, Y. Liu, G. Zhu, X. Xu and K. Chen, *Carbon*, 2012, **50**, 2337-2346.
30. D. R. Dreyer, S. Park, C. W. Bielawski and R. S. Ruoff, *Chem Soc Rev*, 2010, **39**, 228-240.
31. D. Sun, Q. Zou, G. Qian, C. Sun, W. Jiang and F. Li, *Acta Mater*, 2013, **61**, 5829-5834.

32.　　M.-H. Tsai, I. H. Tseng, Y.-F. Liao and J.-C. Chiang, *Polym Int*, 2013, **62**, 1302-1309.
33.　　C. Mattevi, G. Eda, S. Agnoli, S. Miller, K. A. Mkhoyan, O. Celik, D. Mastrogiovanni, G. Granozzi, E. Garfunkel and M. Chhowalla, *Adv Funct Mater*, 2009, **19**, 2577-2583.
34.　　W.-S. Ma, J. Li, B.-J. Deng and X.-S. Zhao, *J Mater Sci*, 2013, **48**, 156-161.
35.　　A. Gupta, A. P. Singh, S. Varshney, N. Agrawal, P. Sambyal, Y. Pandey, B. P. Singh, V. N. Singh, B. K. Gupta and S. K. Dhawan, *Rsc Advances*, 2014, **4**, 62413-62422.
36.　　L. Cao, Q. Sun, H. Wang, X. Zhang and H. Shi, *Composites Part A: Applied Science and Manufacturing*, 2015, **68**, 140-148.
37.　　Y.-L. Li, C.-F. Kuan, C.-H. Chen, H.-C. Kuan, M.-C. Yip, S.-L. Chiu and C.-L. Chiang, *Mater Chem Phys*, 2012, **134**, 677-685.
38.　　X. Yang, X. Wang, J. Yang, J. Li and L. Wan, *Chem Phys Lett*, 2013, **570**, 125-131.
39.　　D. Sarkar, A. Bhattacharya, P. Nandy and S. Das, *Mater Lett*, 2014, **120**, 259-262.
40.　　S. Sutradhar, S. Das and P. K. Chakrabarti, *Mater Lett*, 2013, **95**, 145-148.
41.　　C. Wang, X. Han, P. Xu, J. Wang, Y. Du, X. Wang, W. Qin and T. Zhang, *The Journal of Physical Chemistry C*, 2010, **114**, 3196-3203.
42.　　J. Zhu, H. Gu, Z. Luo, N. Haldolaarachige, D. P. Young, S. Wei and Z. Guo, *Langmuir*, 2012, **28**, 10246-10255.
43.　　M.-S. Cao, W.-L. Song, Z.-L. Hou, B. Wen and J. Yuan, *Carbon*, 2010, **48**, 788-796.
44.　　P. A. Miles, W. B. Westphal and A. Von Hippel, *Rev Mod Phys*, 1957, **29**, 279-307.
45.　　C. Hu, Z. Mou, G. Lu, N. Chen, Z. Dong, M. Hu and L. Qu, *Phys Chem Chem Phys*, 2013, **15**, 13038-13043.
46.　　P. Liu, Y. Huang and X. Zhang, *Compos Sci Technol*, 2015, **107**, 54-60.
47.　　S. Zhang, Q. Jiao, J. Hu, J. Li, Y. Zhao, H. Li and Q. Wu, *J Alloy Compd*, 2015, **630**, 195-201.
48.　　G. Giovannetti, P. A. Khomyakov, G. Brocks, V. M. Karpan, J. van den Brink and P. J. Kelly, *Phys Rev Lett*, 2008, **101**.

Figure 1. Schematic representation of the controllable synthesis of rGO/APTS–NZCF nanocomposite.

Figure 2. C 1s XPS spectra of (a) GO and (b) rGO.

Figure 3. XRD patterns of rGO, pure NZCF and rGO/APTS–NZCF nanocomposite.

Figure 4. (a) FT-IR spectra of pure NZCF, APTS–NZCF and rGO/APTS–NZCF nanocomposite, and (b) elemental analysis of APTS–NZCF and rGO/APTS–NZCF.

Figure 5. TG curves of NZCF, rGO and rGO/APTS–NZCF.

Figure 6. (a) Typical magnetic adsorption of the composites dispersed in ethanol, FE-SEM images of (b) rGO nanosheet, (c) pure NZCF, (d) APTS–NZCF particle and (e) rGO/APTS–NZCF nanocomposite, and (f) EDS spectrum of the APTS–NZCF particle.

Figure 7. TEM images of (a) rGO and (b) rGO/APTS–NZCF nanocomposite.

Figure 8. Magnetization curves of NZCF particles and rGO/APTS–NZCF nanocomposites.

Figure 9. Frequency dependence of (a) the real part and (b) imaginary part of the complex permittivity, (c) dielectric loss tangent, (d) the real part and (e) imaginary part of the complex permeability and (f) magnetic loss tangent of the samples.

Figure 10. (a) The variation of reflection loss curves of samples in the frequency range of 2–18 GHz with the thickness of 2 mm, and (b) three-dimensional representation of reflection loss of the rGO/APTS–NZCF nanocomposite with different thickness in the frequency range of 2–18 GHz.

Figure 11. C_0 values of the rGO/APTS–NZCF nanocomposite.
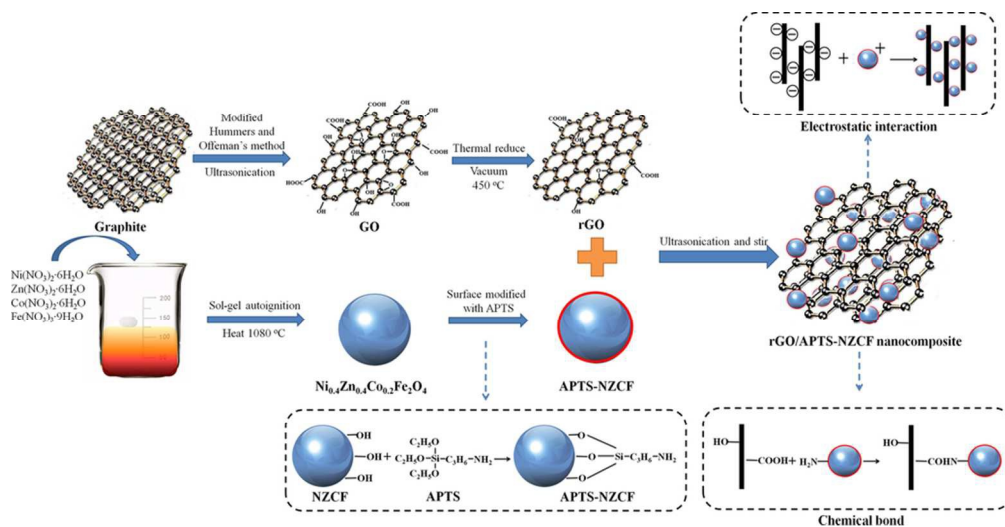
Figure 1. Schematic representation of the controllable synthesis of rGO/APTS−NZCF nanocomposite.
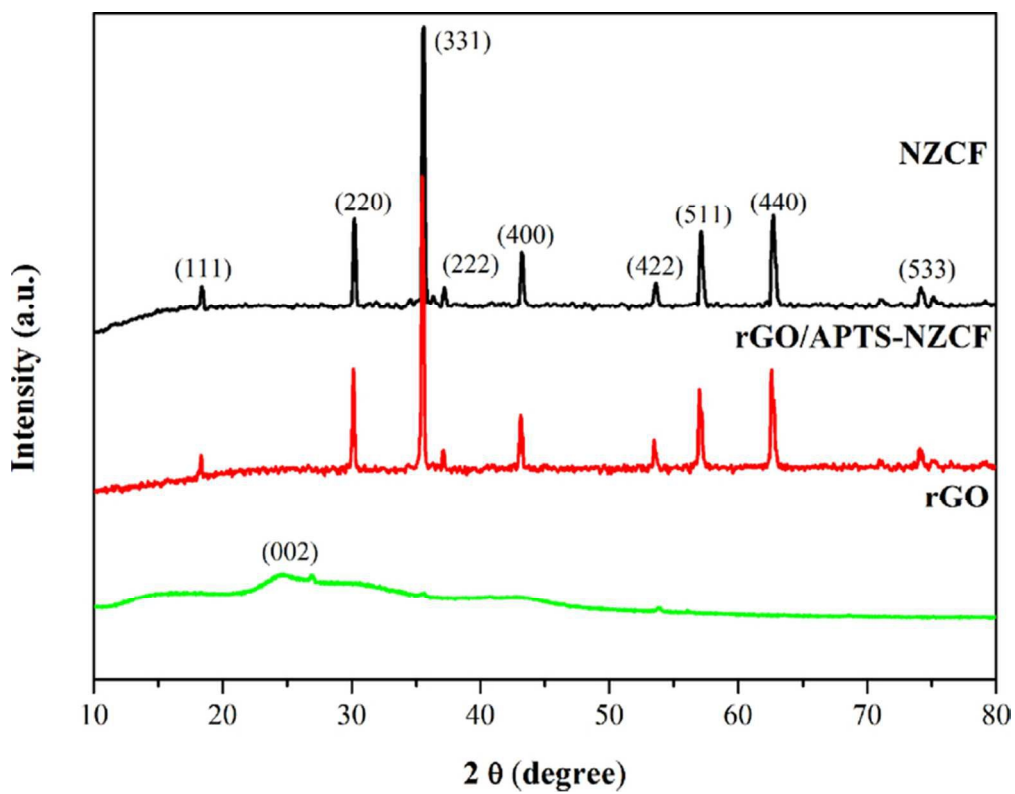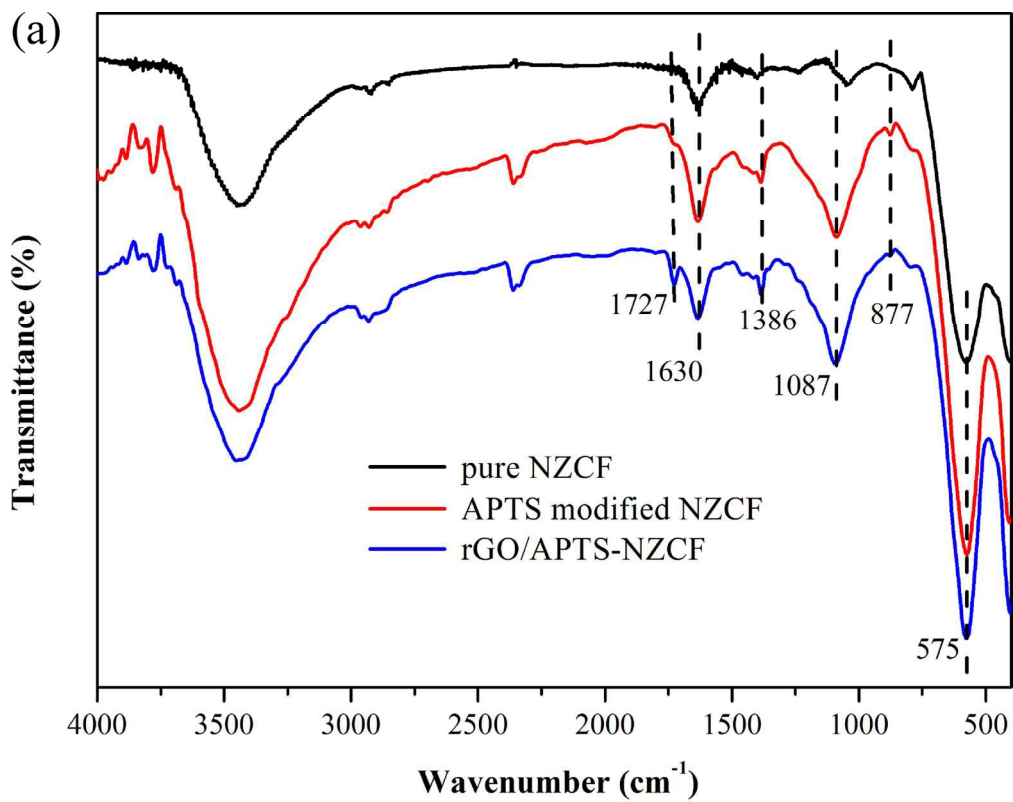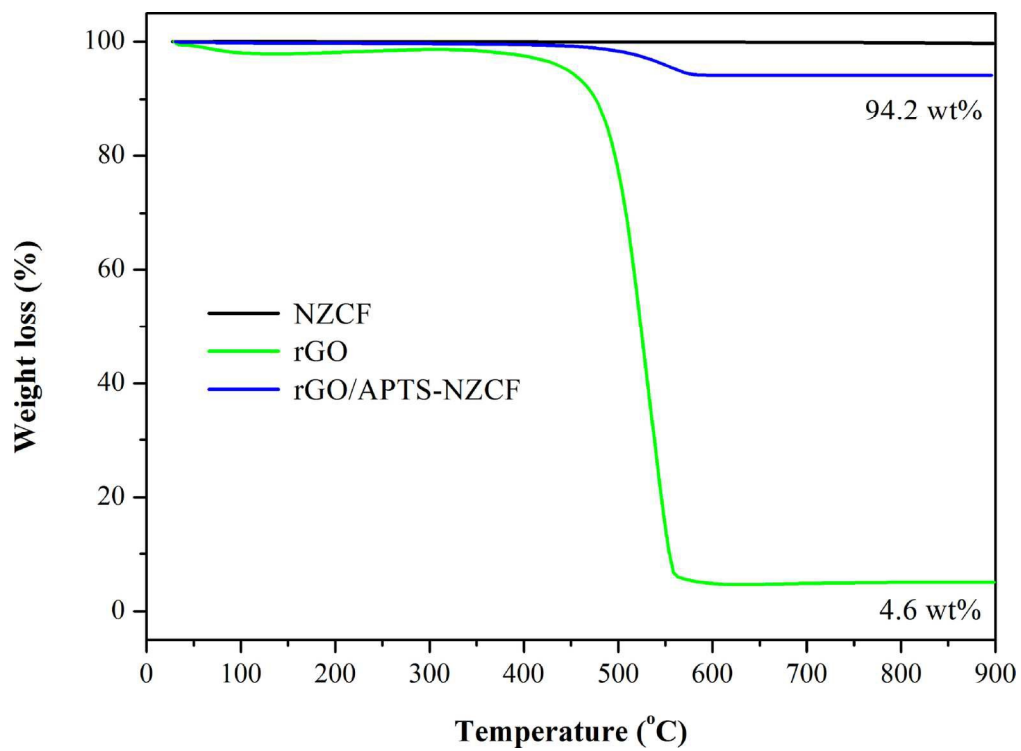87x45mm (300 x 300 DPI)
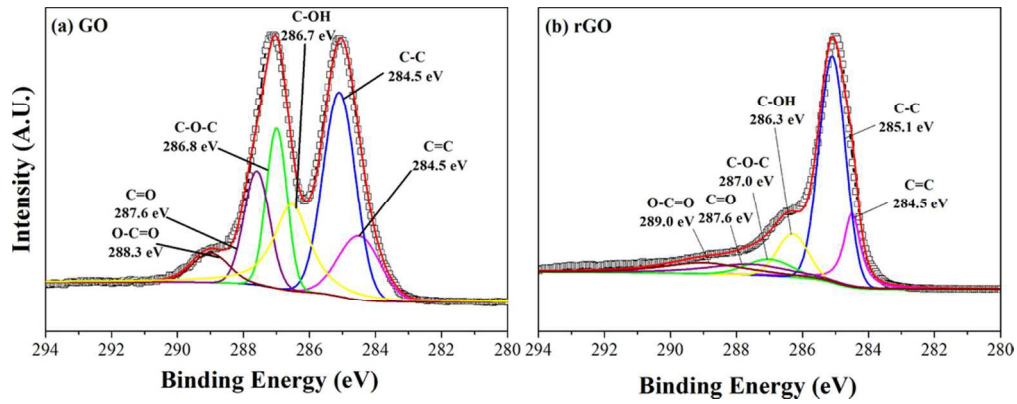
46x18mm (600 x 600 DPI)

Figure 3. XRD patterns of rGO, pure NZCF and rGO/APTS–NZCF nanocomposite.
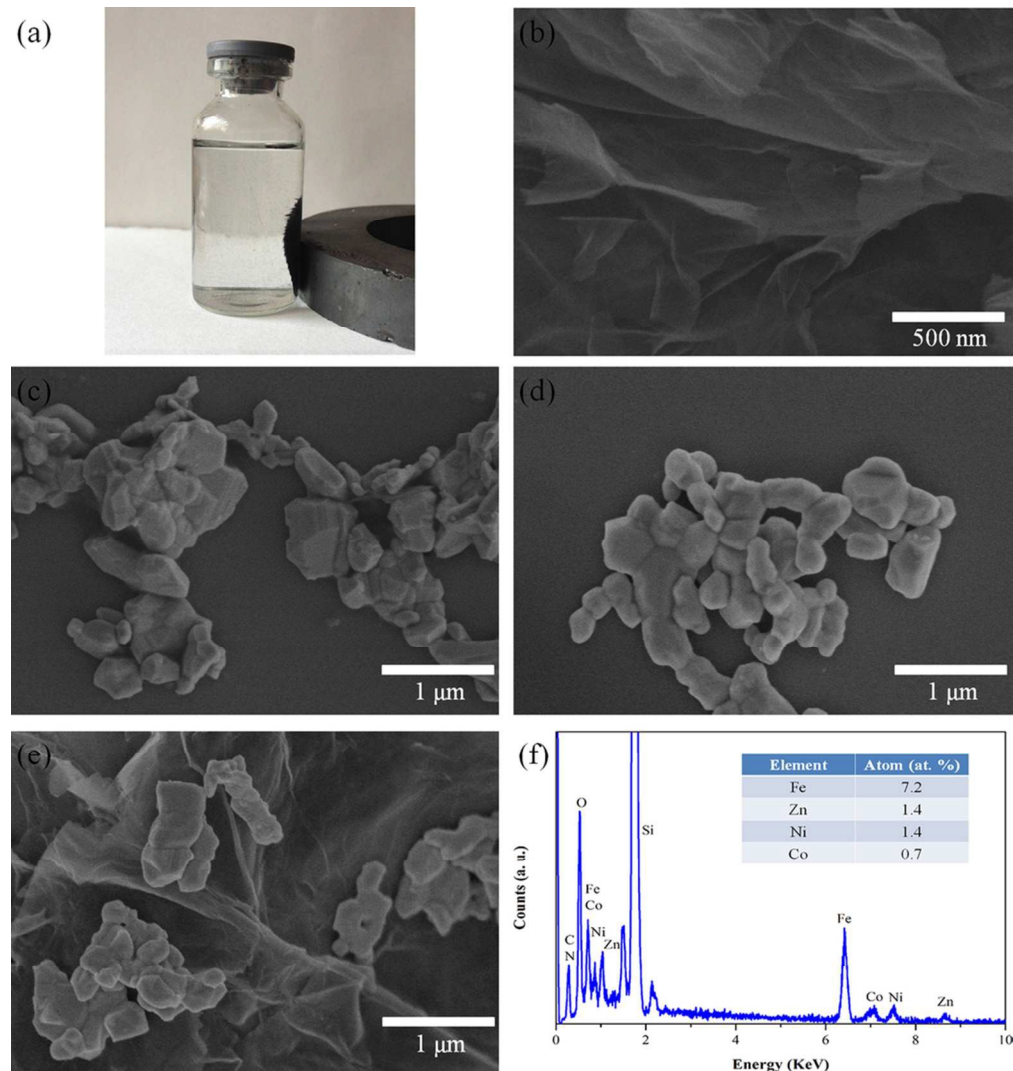64x50mm (300 x 300 DPI)

(a)

(b)

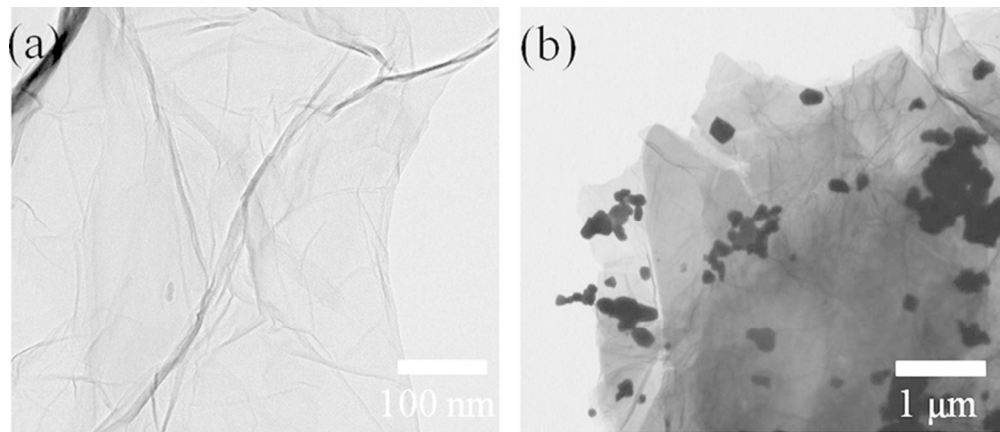| Elemental analysis (wt%)			
	N	C	H
APTS-NZCF	0.2635	0.5500	0.0245
rGO/APTS-NZCF	0.2816	5.8960	0.0790

160x182mm (300 x 300 DPI)
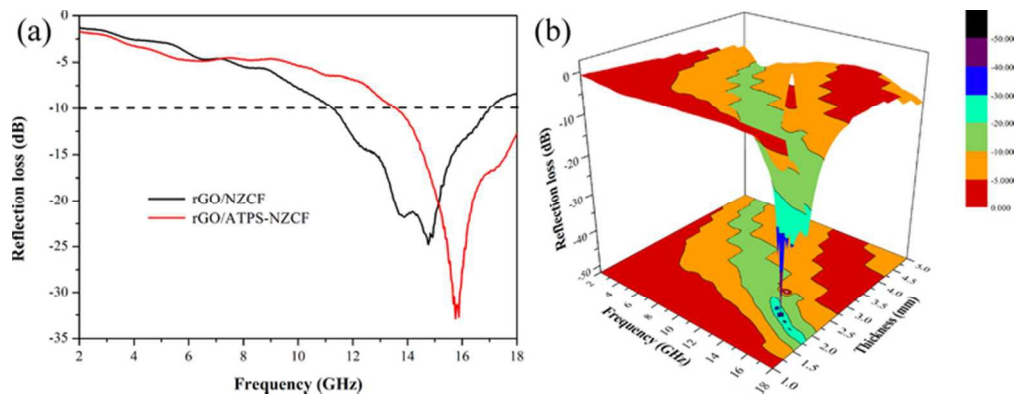
73x53mm (600 x 600 DPI)
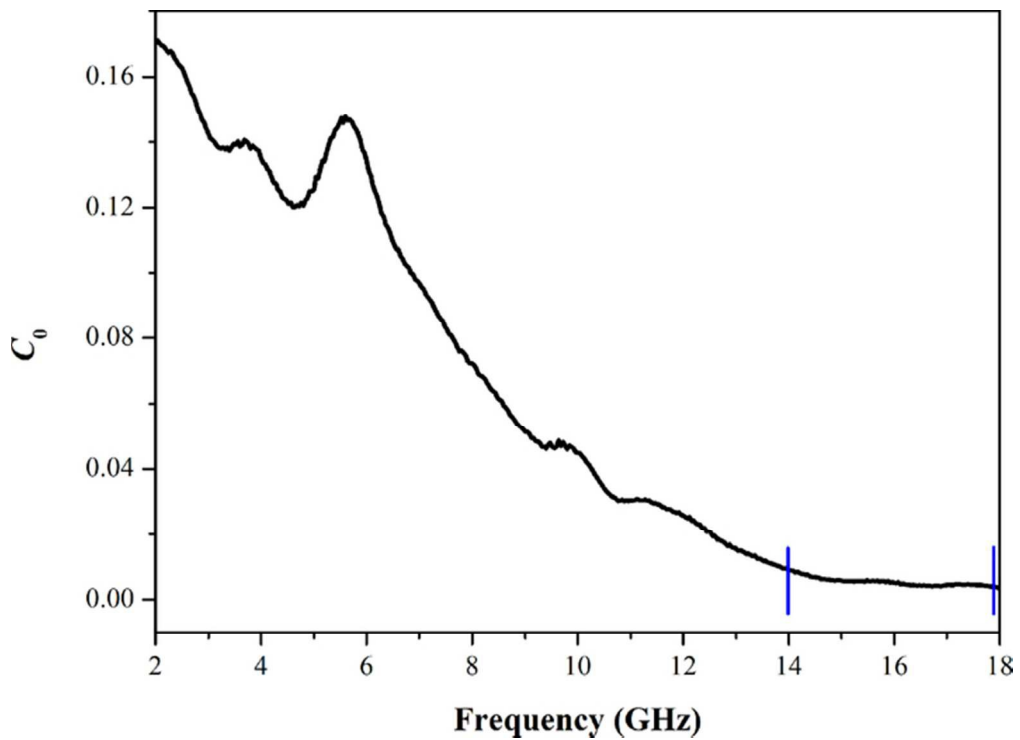
88x94mm (300 x 300 DPI)

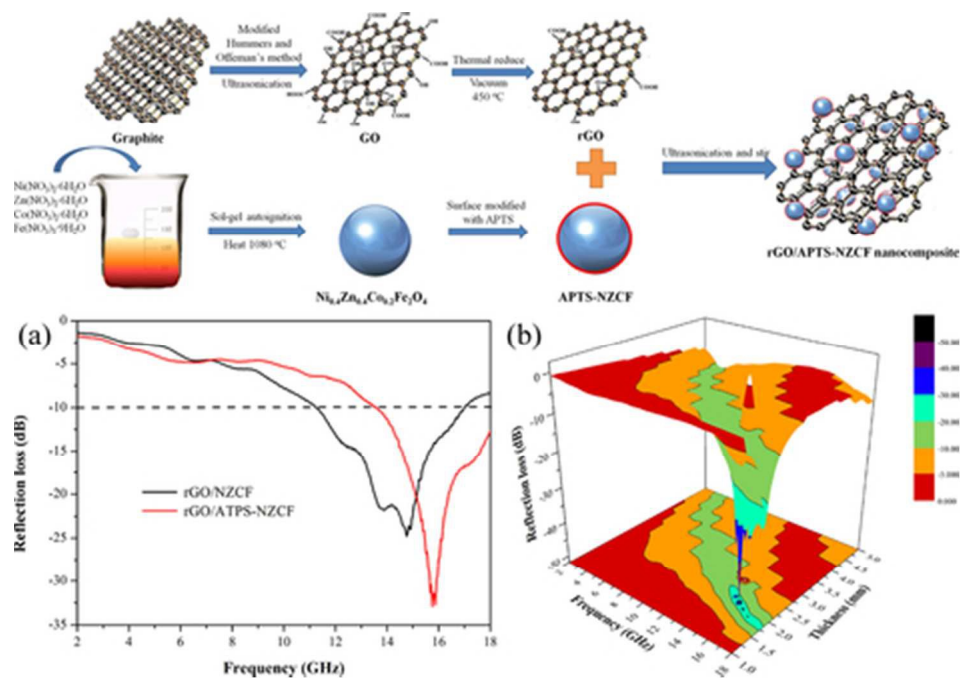72x31mm (300 x 300 DPI)
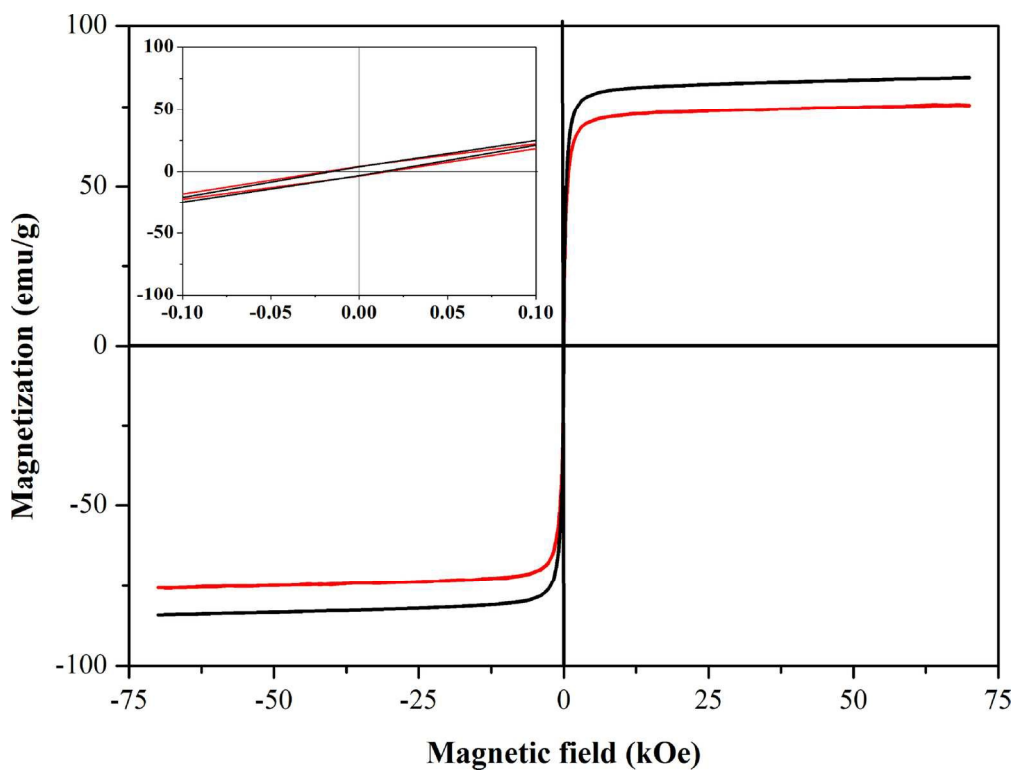
75x56mm (600 x 600 DPI)
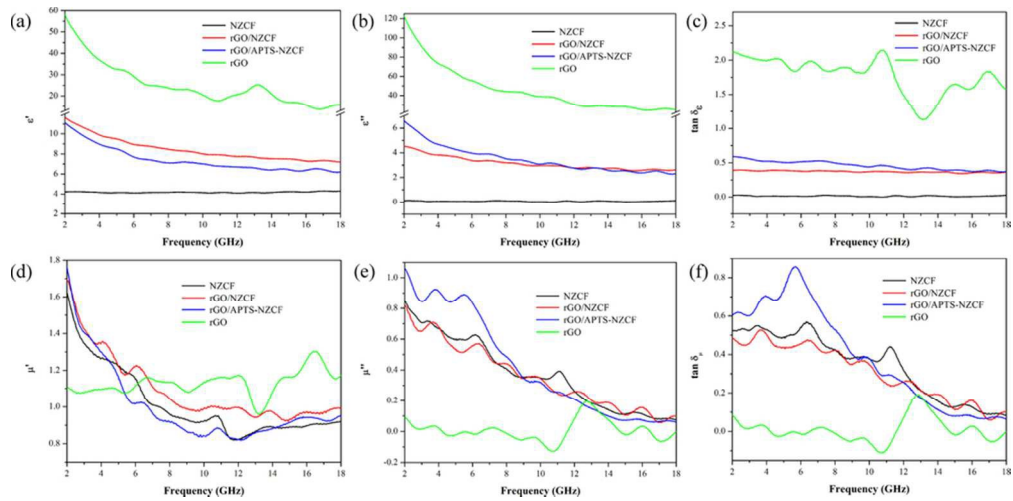
83x41mm (300 x 300 DPI)

65x24mm (300 x 300 DPI)

60x43mm (300 x 300 DPI)

Silane coupling agent modified Ni0.4Zn0.4Co0.2Fe2O4 ferrite decorated reduced graphene oxide nanocomposites were firstly synthesized, and their extraordinary microwave adsorption properties were investigated.
39x28mm (300 x 300 DPI)